Solution and Solid-State Spectra of Quinacridone Derivatives as Viewed from the Intermolecular Hydrogen Bond

Jin Mizuguchi* and Takatoshi Senju

Department of Applied Physics, Graduate School of Engineering, Yokohama National University, 79-5 Tokiwadai, Hodogaya-ku, 240-8501 Yokohama, Japan

Received: February 13, 2006; In Final Form: June 22, 2006

Quinacridones are industrially important hydrogen-bonded pigments. The color in the solid state is vivid red, while it is pale yellow in solution, indicating evidently the involvement of intermolecular interactions in the solid state. The electronic structure has therefore been investigated with special attention to the role of intermolecular NH···O hydrogen bonds for three representative quinacridone compounds with different hydrogen-bond forming characteristics: unsubstituted γ-quinacridone (γ-QA) with two NH groups, mono-*N*-methylquinacridone (MMQA) with one NH and one CH_3, and *N*,*N*′-dimethyl-quinacridone (DMQA) with two CH_3 groups. The number of the NH···O hydrogen bonds per molecule is four, two, and zero for γ-QA, MMQA, and DMQA, respectively. In solution, no significant difference in absorption maximum is recognized between γ-QA, MMQA, and DMQA. However, in the solid state, the absorption maximum of γ-QA appears at the longest wavelength, followed by MMQA and then DMQA, depending on the number of NH···O intermolecular hydrogen bonds. The role of the hydrogen bond is found to align transition dipoles in a "head-to-tail" fashion and to displace the absorption band toward longer wavelengths due to excitonic interactions. The extent of the spectral shift increases with increasing number of hydrogen bonds per molecule.

1. Introduction

Quinacridones (QAs) are industrially important red colorants which belong to the class of hydrogen-bonded pigments that includes indigos and diketopyrrolopyrroles (DPPs).[1] Among QA products, unsubstituted γ-quinacridone (γ-QA) and 2,9-dimethylquinacridone enjoy widespread use in painting and imaging industries due to their high tinctorial strength and outstanding light and heat fastness. The hydrogen-bonded pigments are characterized by NH···O intermolecular hydrogen bonds between the NH group of one molecule and the O atom of the neighboring one that hold molecules firmly together. Thus, the hydrogen bond imparts a polymer-like stability to these compounds. Other characteristic features are that the QA molecule is small (molecular weight of ∼300) and is almost colorless in solution. Nevertheless, they exhibit a vivid red color in the solid state. This clearly indicates that intermolecular interactions are deeply involved in the color generation in the solid state.

Previously, we were involved in the problem of large spectral shifts of DPP[2−4] and indigo[5] on going from solution to the solid state on the basis of the crystal structure from the standpoint of intermolecular hydrogen bonds. We have interpreted the bathochromic displacement in terms of excitonic interactions between transition dipoles where the NH···O intermolecular hydrogen bonds align the transition dipoles in a "head-to-tail" fashion which maximizes the spectral shift. In the present investigation, we aim at elucidating the electronic structure of QA pigments, again with major focus on the intermolecular hydrogen bonds. For this investigation, we have selected three kinds of QA compounds with different hydrogen-bond forming characteristics: unsubstituted γ-quinacridone (γ-QA) with two NH groups, mono-*N*-methylquinacridone (MMQA) with one NH and one CH_3, and *N*,*N*′-dimethyl-quinacridone (DMQA) with two CH_3 groups (Figure 1). The number of the NH···O intermolecular hydrogen bonds per molecule is four, two, and zero for γ-QA, MMQA, and DMQA, respectively. In DMQA, the major intermolecular interactions are van der Waals ones, whereas the hydrogen-bond interactions are additionally operative in MMQA and γ-QA.

In the present paper, we begin with the problem of spectral shifts in solution due to the formation of hydrogen bonds with various solvents and also due to deprotonation at the NH group in MMQA and QA by means of an alkali ($>NH + OH^- \rightarrow >N^- + H_2O$). Then, we discuss the spectral displacement on going from solution to the solid state in terms of the molecular exciton theory of Kasha[6] based on dimeric molecules: A and B. Upon crystallization, the ground-state interaction as well as the excited-state one will appear in the form of $\langle AB|V|AB\rangle$ and $\langle A^*B|V|A^*B\rangle$ (or $\langle AB^*|V|AB^*\rangle$), respectively, where *V* denotes the intermolecular perturbation potential and the molecule with an asterisk (*) designates the excited molecule. The former is called van der Waals interaction in the ground state, while the latter, that in the excited state. The difference in both van der Waals terms corresponds to a bathochromic shift (energy lowering) upon crystallization. This term is sometimes called "crystal shift". Additional bathochromic or hypsochromic shift arises from excitonic interactions (i.e., interactions between transition dipoles) in the form of $\langle A^*B|V|AB^*\rangle$ (or $\langle AB^*|V|A^*B\rangle$). This interaction prevails in systems where the absorption coefficient (which is proportional to the square of the transition dipole) of the component molecule is quite large, as typical in the case of dyestuffs and pigments.[6,7]

The crystal structures of the γ-phase of QA were determined by Potts et al. using synchrotron radiation ($R = 0.1214$).[8] We have also analyzed the structure by X-rays at 223 K ($R = 0.073$).[9] Both results are basically in good agreement. The

* To whom correspondence should be addressed. Phone/Fax: +81 45 339 3369. E-mail: mizu-j@ynu.ac.jp.

10.1021/jp060915l CCC: $33.50
Published on Web 09/08/2006

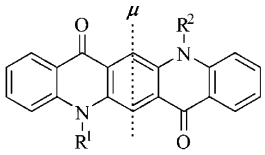

1: QA $R^1=R^2=H$
2: MMQA $R^1=Me, R^2=H$
3: DMQA $R^1=R^2=Me$

Figure 1. Molecular structure of quinacridone derivatives: γ-QA, MMQA, and DMQA. The dotted line denotes the direction of the transition dipole as deduced from molecular orbital calculations (see text).

structure of MMQA has newly been determined by us in the present investigation.[10] On the other hand, the crystal structure of DMQA has variously been reported by Ohmasa et al. ($R_1 = 0.15$ for 726 nonzero reflections),[11] Zavodnik et al. ($R = 0.047$ for 532 reflections with $I > 3\sigma$),[12] and also by us ($R_1 = 0.044$ for 1349 reflections with $I > 2\sigma$).[13]

2. Experimental Section

2.1. Materials and Sample Preparations. QA was obtained from Ciba Specialty Chemicals. MMQA and DMQA were synthesized according to the method described in the literature.[14] The samples were purified twice by sublimation, using a two-zone furnace.[15] Single crystals of QA and DMQA were grown from solution in dimethylformamide using an autoclave, whereas single crystals of MMQA were grown from the vapor phase at about 583 K.

2.2. Equipment and Measurements. UV−vis spectra in solution were recorded on a UV-2400PC spectrophotometer (Shimadzu). Measurements for polarized reflection spectra were made on single crystals by means of a UMSP80 microscope spectrophotometer (Carl Zeiss). An Epiplan Pol (×8) objective was used together with a Nicol-type polarizer. Reflectivities were corrected relative to the reflection standard of silicon carbide. Fourier transform infrared (FT-IR) reflection spectra were measured on single crystals by using a microsampling FT-IR instrument (model MFT-2000) from JASCO.

TGA/DTA (thermogravimetric analysis and differential thermal analysis) measurements were made on powdered samples under vacuum by means of a Thermo Plus 2 TG-8130 instrument from Rigaku at a heating rate of 10 °C/min. ^{1}H NMR (at 400 MHz) spectra were recorded with a JNM-AL400 spectrometer from JEOL.

Deprotonation experiments were carried out by adding a small amount of 0.1 N TBAH (tetrabutylammonium hydroxide) to a QA solution in dimethyl sulfoxide (DMSO) under argon (degassed) while monitoring the absorption spectra as well as the electric conductivity of the solution ("conductometric titration").

2.3. Molecular Orbital (MO) Calculations. Quantum Cache ver. 3.2[16] used for MO calculations includes MOPAC ver. 94.10 as well as the INDO/S program released by Ridley and Zerner,[17] which is a spectroscopically calibrated semiempirical MO method. Geometry was optimized for QA, MMQA, and DMQA together with their deprotonated states on the basis of the AM1 Hamiltonian in MOPAC ver. 94.10.[16] Then, the Mulliken population analysis was made on the optimized geometry of QA, specifying the keywords "1 SCF" and "MULLIK". The optical absorption bands were also calculated on the optimized geometries using the INDO/S Hamiltonian, using 144 singly excited configuration interactions (CI).[16]

TABLE 1: Crystallographic Parameters for QA, MMQA, and DMQA

	QA[9]	MMQA[10]	DMQA[13]
formula	$C_{20}H_{12}N_2O_2$	$C_{21}H_{14}N_2O_2$	$C_{22}H_{16}N_2O_2$
crystal system	monoclinic	orthorhombic	monoclinic
space group	$P2_1/c$	$Pbca$	$P2_1/c$
Z	2	8	2
molecular weight	312.32	326.35	340.37
molecular symmetry	C_i	C_1	C_i
a (Å)	13.70(1)	13.517(2)	4.928(3)
b (Å)	3.84(1)	7.340(2)	11.103(3)
c (Å)	13.35(2)	29.033(2)	14.462(2)
α (deg)	90	90	90
β (deg)	100.09(9)	90	98.39(2)
γ (deg)	90	90	90
V (Å^3)	691(2)	2880.5(8)	782.8(4)
T (K)	223(2)	93(2)	223(2)
R_1	0.073	0.072	0.044
$wR_{ref}(F^2)$	0.213	0.162	0.126
GOF	1.27	1.15	1.59
d_{calcd} (g/cm^{-3})	1.499	1.505	1.444

3. Results

3.1. Crystal Structure of Quinacridone Derivatives. Table 1 details the crystallographic parameters for γ-QA,[9] MMQA,[10] and DMQA.[13] The molecular arrangement is also shown in Figure 2 for these derivatives.

The molecule of γ-QA is entirely planar and belongs to the point group of C_i. As shown in Figure 2a, there are chains of intermolecular hydrogen bonds along the c-axis between the NH group of one molecule and the O atom of the neighboring one. One molecule is hydrogen-bonded to four different molecules in a "hunter's fence" fashion, leading to the formation of a three-dimensional hydrogen-bond network. This kind of molecular arrangement is typical of indigo[18] and dithioketo-quinacridone pigments.[19] The N/O distance and the NH/O angle are 2.756 Å and 163°, respectively. The present geometry of the hydrogen bond serves often as a good measure of the strength of the hydrogen bond. Strong bonds are typically characterized by a short N/O distance and an NH/O angle of nearly 180°.[20,21]

The MMQA molecule is again entirely planar. A small dipole moment of about 0.36 D appears as a result of C_1 symmetry. Figure 2b shows the projections of the crystal structure onto the (a,c) and (b,c) planes. There are two kinds of stacking columns along the b-axis. The molecules in one column are inclined at about 45° with respect to the molecules in the neighboring column. In each column, the MMQA molecule and its inverted one are stacked pairwise alternately along the b-axis. There is a one-dimensional (chainlike) intermolecular NH···O hydrogen bond along the a-axis. One molecule is hydrogen-bonded to two neighboring molecules. The N/O distance and the NH/O angle are 2.721 Å and 166°, respectively. This hydrogen-bond parameter is quite similar to that of γ-QA.

The molecule of DMQA[13] is entirely planar. The molecules are stacked along the a-axis with significant overlap in a herringbone fashion, as shown in Figure 2c. The space group of the present structure is the same as that of γ-QA ($P2_1/c$), and the lattice parameters and molecular arrangement are relatively similar to each other.

3.2. Molecular Orbital Calculations. The deprotonation reaction of QA or MMQA occurs at the NH site by means of an alkali (>NH + OH$^-$ → >N$^-$ + H$_2$O). Possible structures for the deprotonated QA are shown in Figure 3. Structures **IIb** and **IIIb** are of the full aromatic form and are thus expected to be more stable than **IIa** and **IIIa**, respectively. To clarify this,

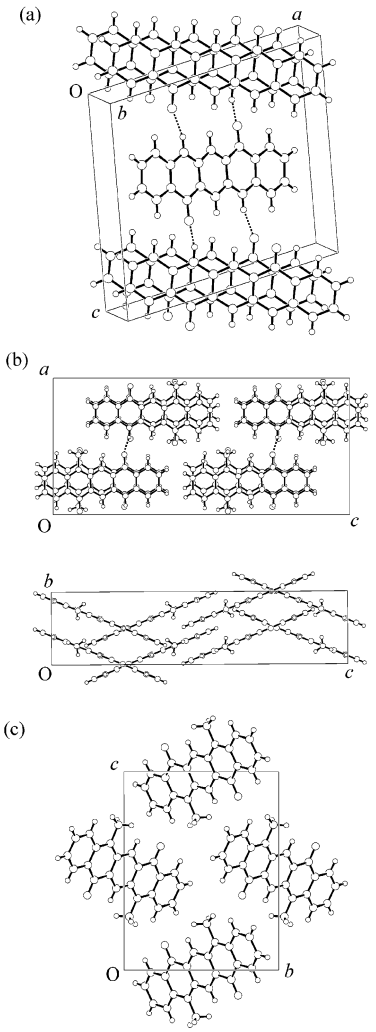

Figure 2. Molecular arrangement: (a) γ-QA; (b) MMQA ((*a*,*c*) and (*b*,*c*) planes); (c) DMQA. The dotted lines designate NH···O intermolecular hydrogen bonds.

the Mulliken pupulation analysis is necessary on the optimized geometry of the mono- and di-deprotonated states, as shown below.

Table 2 details the heat of formation of the optimized geometry as well as spectroscopic calculations for QA and MMQA for the initial and deprotonated states and for DMQA for the initial state. As judged from the heat of formation of the initial, mono-deprotonated, and di-deprotonated states of QA, the mono-deprotonated one is the most stable, followed by the di-deprotonated one and then the initial one. This is closely correlated with the reorganized electron densities on the N and O atoms upon deprotonation, as shown below. Table 3 shows the charge densities of the N and O atoms in QA upon deprotonation calculated by the Mulliken population analysis. In the initial state, the formal charges of the N and O atoms are slightly negative. The mono-deprotonation at nitrogen 1 (N1) brings about a remarkable increase in the "s" charge density (1.611 → 1.841) as well as a significant decrease in the "p_z" density (1.723 → 1.339). As a consequence, this induces a change in charge density of oxygen 1 (O1) located in the same heterocyclic ring in a manner that the "p_z" charge density greatly increases from 1.394 to 1.489. The N2 and O2 are little influenced by the mono-deprotonation. Finally, O1 becomes more negatively charged (−0.319 → −0.427) on mono-deprotonation, whereas no significant change is observed in N1. The di-deprotonation at N2 induces an increase in the "s" charge density (1.611 → 1.839) and a decrease in the "p_z" charge density (1.713 → 1.333). This enhances again the "p_z" charge density of O2 (1.412 → 1.498). It follows that O1 and O2 become more negatively charged (−0.319 → −0.447) on di-deprotonation, whereas the net atomic charges of N1 and N2 remain practically unchanged. The above consideration supports the fact that the structures **IIb** and **IIIb** in Figure 3 are dominant upon mono- and di-deprotonations, respectively. A similar result was also obtained for MMQA in the deprotonated state.

Spectroscopic calculations revealed that there is only one electronic transition in the visible region in QA, MMQA, and DMQA assigned to the HOMO/LUMO $\pi-\pi^*$ transition. The direction of the transition dipole (μ) in QA compounds points perpendicular to the long-molecular axis, as shown in Figure 1. In the initial state, no significant difference in absorption maximum as well as in oscillator strength is recognized between QA, MMQA, and DMQA. The absorption maximum of QA is then displaced appreciably toward longer wavelengths due to mono-deprotonation and less significantly due to di-deprotonation. The same spectral shift is also observed in MMQA. This is well understood because the negative charge at the $>N^-$ site can be delocalized throughout the chromophore to displace the absorption band toward longer wavelengths.

3.3. Solution Spectra. Figure 4 shows the solution spectrum in dimethyl sulfoxide (DMSO) for QA. MMQA and DMQA gave almost the same spectra and thus were omitted. A beautiful progression of the absorption bands was observed starting from about 523 nm. Since the longest-wavelength band is quite steep and the absorption bands are equally spaced, this band is assigned to the pure electronic transition 0−0 and the second-longest-wavelength band to the 0−1, and so forth, as shown in Figure 4, indicating that one single electronic transition is coupled with vibrational transitions. This result is also in accord with the MO calculations.

Figure 5a shows the solution spectra of QA measured in DMSO, dimethylformamide (DMF), and 1,4-dioxane. Bathochromic shifts are noticed in DMF and DMSO relative to the corresponding spectrum in 1,4-dioxane. The spectral shift is 10 nm (about 373 cm^{-1}) in DMF and 16 nm (about 603 cm^{-1}) in DMSO, and the extent of the shift follows the relative order of increasing polarity of the solvents. The temperature dependence of the absorption spectra of QA in DMSO is shown in Figure 5b. A hypsochromic displacement is observed as the temperature is raised. The present phenomenon is closely related to the intermolecular hydrogen bond between solute and solvent as described below.

The same tendency is also observed in MMQA.

3.4. ^{1}H NMR Spectra. Table 4 shows the proton chemical shifts of the NH group of QA in DMSO as a function of temperature. The chemical shifts appear around 12 ppm which is characteristic of the hydrogen-bonded proton. This is due to the NH···O intermolecular hydrogen bond between the NH group of QA and the O atom of DMSO. The present chemical shift decreases with increasing temperature, indicating that the hydrogen bond is substantially weakened at high temperatures because of the enhanced kinetic motion of molecules. This behavior is well correlated with the temperature dependence of absorption spectra shown in Figure 5b.

3.5. Conductometric Titration and Deprotonation Experiment. Figure 6 shows the specific conductivity of the QA solution in DMSO plotted against the molar ratio of TBAH to QA. The conductivity of the solution increases linearly from the commencement of the titration. This represents the ionization

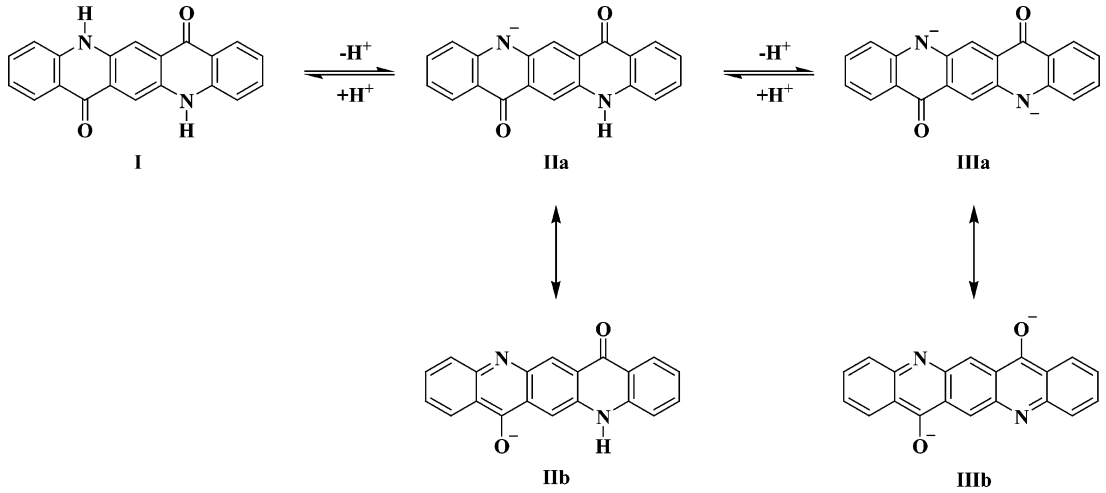

Figure 3. Deprotonation of QA and possible mono- and di-deprotonated structures.

TABLE 2: Heat of Formation and Calculated Absorption Bands for QA, MMQA, and DMQA

compound	state	H_f (kcal/mol)	λ (nm)	oscillator strength
QA	initial	24.93	373.3	0.2772
QA	mono-deprotonated	−14.23	477.8	0.1541
QA	di-deprotonated	10.97	461.7	0.3416
MMQA	initial	33.91	376.1	0.2744
MMQA	mono-deprotonated	−4.02	490.6	0.1309
DMQA		44.63	379.5	0.2783

TABLE 3: Mulliken Population Analysis (MPA) and Net Atomic Charges (NACs) for the N and O Atoms of QA in the Initial, Mono-deprotonated, and Di-deprotonated States

			state		
atom[a]			initial	mono-deproto.	di-deproto.
nitrogen 1 (N1)	MPA	s	1.611	1.841	1.839
		p_x	0.992	0.908	0.920
		p_y	1.070	1.239	1.242
		p_z	1.723	1.339	1.333
	NAC		−0.254	−0.294	−0.300
nitrogen 2 (N2)	MPA	s	1.611	1.611	1.839
		p_x	0.992	1.008	0.920
		p_y	1.070	1.052	1.242
		p_z	1.723	1.713	1.333
	NAC		−0.254	−0.243	−0.300
oxygen 1 (O1)	MPA	s	1.972	1.970	1.969
		p_x	1.834	1.843	1.852
		p_y	1.143	1.148	1.152
		p_z	1.394	1.489	1.498
	NAC		−0.319	−0.427	−0.447
oxygen 2 (O2)	MPA	s	1.972	1.971	1.969
		p_x	1.834	1.849	1.852
		p_y	1.143	1.141	1.152
		p_z	1.394	1.412	1.498
	NAC		−0.319	−0.348	−0.447

[a] The mono-deprotonation takes place at the N1 atom in the one heterocyclic ring in which O1 is situated, whereas N2 and S2 lie in the other ring.

of the acid (QA) and the replacement by its salt which is a strong electrolyte. From point A, the conductivity increases with a higher gradient up to point B. The linear increase after point B is attributed to the intrinsic conductivity of TBAH in DMSO. Point A corresponds exactly to the half equivalent of QA, and point B, to the equivalent point. This indicates that the first deprotonation is completed at point A and the second at point B.

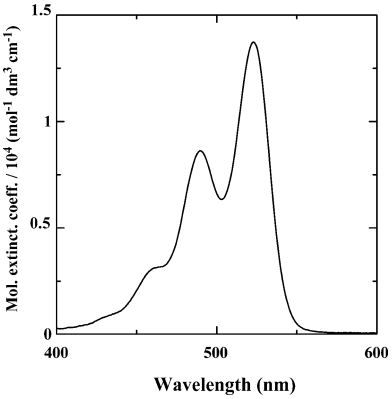

Figure 4. Solution spectrum of QA in DMSO. No noticeable difference in absorption position as well as spectral shape is observed between the spectra of QA, MMQA, and DMQA. The molar extinction coefficient of QA, MMQA, and DMQA should be multiplied by 1.0, 1.05, and 1.04, respectively.

The absorption spectra from the initial point to point A are shown in Figure 7a, whereas those between points A and B are given in Figure 7b. Three isosbestic points are noticed in both figures which indicates that the spectral changes may be based on a binary equilibrium system: undeprotonated and mono-deprotonated species in Figure 7a and mono and di-deprotonated species in Figure 7b. In fact, the deprotonation reaction is fully reversible, as shown by the fact that the addition of, for example, hydrochloric acid regenerates the initial state. The absorption maximum of the mono-deprotonated species gives a maximum at 610.5 nm. Di-deprotonation brings about a further bathochromic shift, up to 658 nm (Figure 7b), but the extent of the bathochromic shift in di-deprotonation is less intensive as compared with that in mono-deprotonation. The present spectral displacement as well as the extent of the spectral shift is qualitatively in good agreement with the MO calculations described above. It should also be noted that the spectral shapes of the deprotonated species (especially that of mono) are very similar to that of QA. This indicates that the deprotonation merely displaces the absorption spectrum to the longer wavelengths by about 87−135 nm (∼2727−3923 cm^{-1}).

The deprotonation behavior of MMQA proceeds exactly in the same way as that of QA. The absorption maximum of the deprotonated MMQA occurs nearly at the same wavelength as that of mono-deprotonated QA.

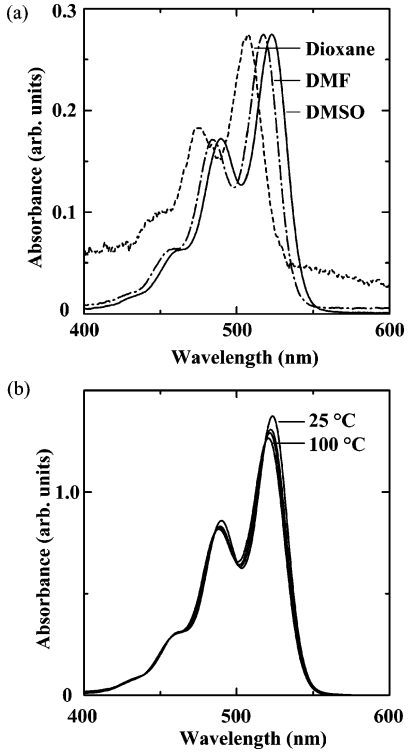

Figure 5. (a) Solution spectra of QA in 1,4-dioxane, DMF, and DMSO and (b) the temperature dependence of the solution spectra of QA in DMSO measured at 25, 50, 75, and 100 °C.

TABLE 4: Temperature Dependence of ^{1}H NMR Chemical Shift for the Proton of the NH Group in QA

temperature (°C)	chemical shift (ppm)
25	11.83
50	11.73
75	11.62
100	11.51

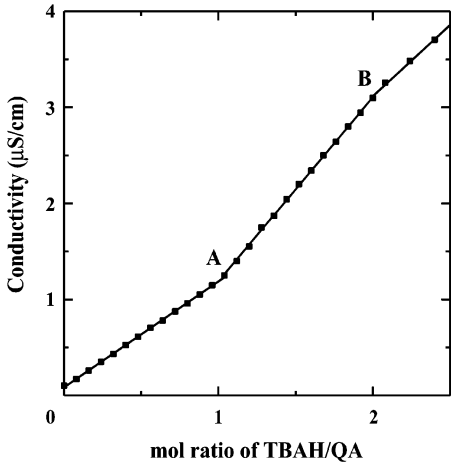

Figure 6. Conductometric titration of QA/DMSO solution (8.7×10^{-4} M; 100 mL) with TBAH. Points A and B denote the first and second end points, respectively.

3.6. TGA Measurements. Figure 8 shows the weight loss of γ-QA, MMQA, and DMQA as a function of temperature. DMQA begins to sublime at about 175 °C, followed by MMQA at about 275 °C and then by γ-QA at about 330 °C. This result indicates that intermolecular forces become stronger in the order of DMQA, MMQA, and QA, and the NH···O intermolecular forces contribute greatly to the cohesion of the crystal lattice in MMQA and more significantly in γ-QA.

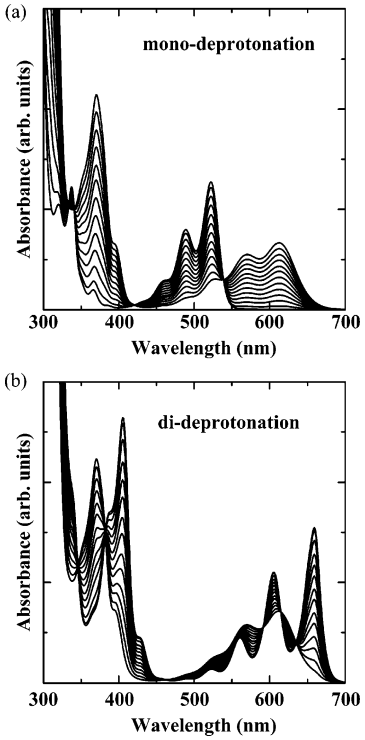

Figure 7. Solution spectra of QA in DMSO as a function of the molar ratio of TBAH to QA: (a) up to point A in Figure 6 (molar ratio = 1:1); (b) between points A and B in Figure 6 (molar ratio = 1:2).

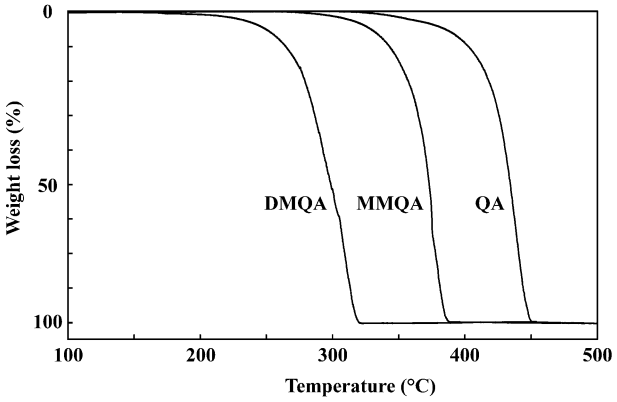

Figure 8. TGA measurements for DMQA, MMQA, and QA. Weight loss is plotted as a function of temperature.

3.7. Polarized Reflection Spectra Measured on Single Crystals. Figure 9 shows the polarized reflection spectra measured on the (100) plane of QA single crystals together with the molecular arrangement. A prominent reflection band appears around 565 nm together with two small bands around 491 and 527 nm for polarization parallel to the direction of the NH···O intermolecular hydrogen bond, as designated by the dotted line in Figure 9b. On the other hand, these bands are completely quenched for polarization perpendicular to this direction. This clearly indicates that all the reflection bands belong to one single electronic transition and that the direction of the transition dipole points along the intermolecular hydrogen bond. The present result is also borne out by the MO calculation which shows that there is only one electronic transition in the visible region and that the direction of the transition dipole appears along the intermolecular hydrogen bond. Then, it follows that the longest-wavelength band (around 572 nm), the second-longest band (around 527 nm), and the third-longest band (491 nm) in Figure 9 correspond to the 0−0, 0−1, and 0−2 transitions in solution

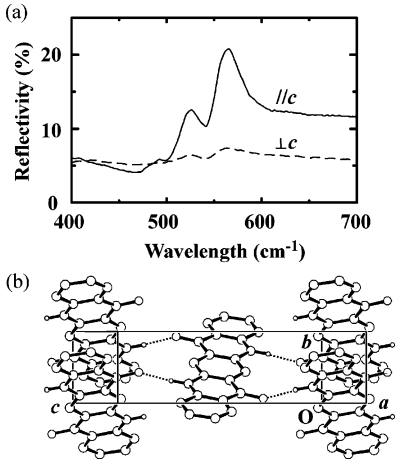

Figure 9. (a) Polarized reflection spectra measured on the (100) plane of γ-QA and (b) the molecular arrangement. The dotted line designates the direction of the intermolecular NH···O hydrogen bond.

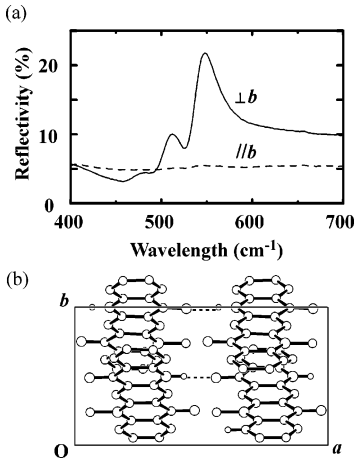

Figure 10. (a) Polarized reflection spectra measured on the (001) plane of MMQA and (b) the projection of the crystal structure onto the (*a*,*b*) plane. The dotted line designates the direction of the intermolecular N−H···O hydrogen bond.

spectra in Figure 4, respectively. The present one-to-one correspondence between solution and solid-state spectra indicates that there is a large bathochromic shift (523 → 565 nm) on going from solution to the solid state in γ-QA.

Likewise, Figure 10 shows the polarized reflection spectra of MMQA measured on the (*a*,*b*) plane for polarization parallel and perpendicular to the *b*-axis. Here again, a strong band occurs at about 548 nm together with two small bands around 478 and 512 nm for polarization perpendicular to the *b*-axis. The transition dipole lies again along the NH···O intermolecular hydrogen bond.

Similarly, DMQA shows the strongest, longest-wavelength band around 538 nm together with two additional bands around 472 and 504 nm (Figure 11). The transition dipole points along the direction perpendicular to the long-molecular axis.

In summary, the direction of the transition dipole in γ-QA, MMQA, and DMQA points along the direction perpendicular to the long-molecular axis, and this is the direction of the NH···O hydrogen bond in γ-QA and MMQA. Furthermore, the reflection maximum expressed in wavelength decreases with decreasing number of NH···O hydrogen bonds. This indicates that the hydrogen bond plays an important role in the spectral

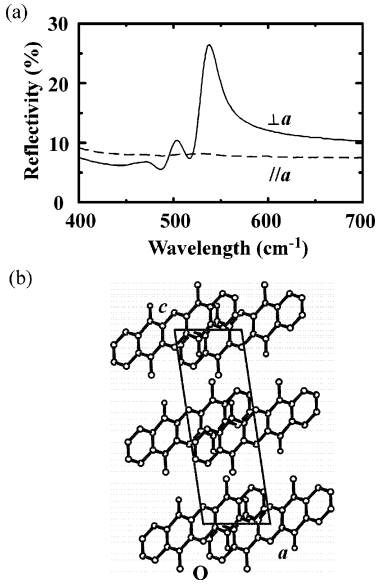

Figure 11. (a) Polarized reflection spectra measured on the (010) plane of DMQA and (b) the projection of the crystal structure onto the (*a*,*c*) plane.

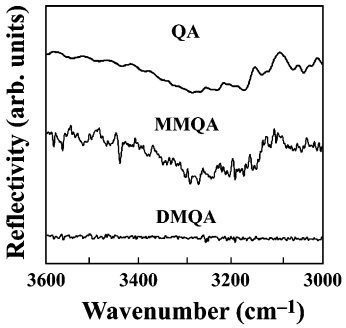

Figure 12. Nonpolarized IR reflection spectra measured on single crystals for QA, MMQA, and DMQA.

shift upon crystallization by aligning the transition dipoles in QA derivatives, as discussed later in section 4.3.

3.8. IR Spectra for QA, MMQA, and DMQA. Figure 12 shows the IR reflection spectra of γ-QA, MMQA, and DMQA measured with unpolarized light on single crystals in the wavenumber region between 3000 and 3600 cm^{-1}. The bands around 3140 cm^{-1} in both QA and MMQA are assigned to the NH stretching vibration, while there is no corresponding band in DMQA. In addition, the position of these NH stretching bands occurs nearly at the same wavenumbers. The present NH stretching bands are broad and displaced toward lower wavenumbers as compared with that of the free NH stretching which appears normally at about 3500 cm^{-1}. This is due to the formation of NH···O intermolecular hydrogen bonds. Furthermore, the strength of the hydrogen bond seems to be of the same magnitude as judged from the same absorption position of the NH stretching band. This is fully consistent with the X-ray geometry consideration of the NH···O hydrogen bond in QA and MMQA that exhibits practically the same parameters of the hydrogen bond (see section 3.1).

4. Discussion

4.1. Increase in Electron Density in the Chromophore due to the Hydrogen Bond with Solvents and Also due to Deprotonation at the NH Group. The ^{1}H NMR chemical shift

of QA in DMSO and its temperature dependence indicates the presence of intermolecular hydrogen bonds between solute and solvent (Table 4). Furthermore, the solvent and temperature effects of QA have also shown that the bathochromic shift in the visible region becomes more significant as the intermolecular hydrogen bond between solute and solvent is intensified (Figure 5a) and that the extent of the spectral shift in QA is reduced as the temperature is raised (Figure 5b). These observations indicate that the intermolecular hydrogen bond brings about spectral displacements, to an extent depending on the strength of the hydrogen bond. This spectral shift can be explained in terms of partial electron transfer from the proton to the nitrogen atom,[21] thereby increasing the electron density on nitrogen. In addition to its primary electrostatic character, the hydrogen bond has some covalent nature corresponding to the scheme $N^{-}-H^{+}\cdots O=C \leftrightarrow N^{-}\ H-O^{+}=C$. This second charge-transfer form involves electron donation from the oxygen into the N−H bond, increasing the electron density on the nitrogen atom. This increased electron density can then be more delocalized into the chromophore in the excited state, contributing to the bathochromic shift.[21]

The hydrogen bond between QA and solvent molecules described above involves a partial electron transfer from the solvent oxygen to the nitrogen ($N^{\delta-}\ H-O^{\delta+}=C$). On the other hand, deprotonation at the NH site in the form of $>N^{-}$ can be pictured as complete electron transfer to the nitrogen atom, accompanied by full delocalization in the entire chromophore. The deprotonation ends up with the reorganization of the electron charge, giving a negative charge on the oxygen atom. This supports the structures **IIb** and **IIIb** in Figure 3.

Deprotonation at the NH group ($>N^{-}$) brings about a large spectral displacement in QA, as shown in Figure 7. The mono- and di-deprotonated species give absorption maxima at 582 and 605 nm, respectively. The difference in displacement energy between the neutral and mono-deprotonated species is ∼2727 cm^{-1}, whereas the mono- and di-deprotonated species give a difference of only ∼1196 cm^{-1}. The present tendency is in good agreement with the result of MO calculations. These observations indicate that the first deprotonation primarily determines the displacement energy, whereas the second one has only a small effect. The present behavior is also in good accord with our previous study on DPP.[2]

4.2. Correlation between NH···O Intermolecular Hydrogen Bonds and Cohesion in the Solid State. As discussed in structure analysis (section 3.1), no significant difference in strength of the NH···O intermolecular hydrogen bond is recognized between QA and MMQA. This is also confirmed by the IR spectra (Figure 12), showing that the extent of the shift of the NH stretching band relative to the free NH band is, more or less, the same. The difference between QA and MMQA is then the number of NH···O intermolecular hydrogen bonds. This is closely related to the difference in cohesion in the solid state as measured by TGA (Figure 8). The sublimation temperature increases characteristically in the order of DMQA, MMQA, and QA, as the number of the NH group in each molecule is increased. This indicates that intermolecular forces are strongly increased with an increase in the number of hydrogen bonds.

Then, we focus on the bathochromic displacement in QA, MMQA, and DMQA on going from solution to the solid state. The spectral shift is 14.5 nm (∼515 cm^{-1}) in DMQA, 25 nm (∼872 cm^{-1}) in MMQA, and 42 nm (∼1421 cm^{-1}) in QA. The shift becomes larger as the number of hydrogen-bonding sites is increased. This suggests that the intermolecular hydrogen bond in the solid state exerts a profound influence on the spectral displacement upon crystallization.

4.3. Spectral Shifts upon Crystallization due to Excitonic Interactions—The Role of NH···O Intermolecular Hydrogen Bonds. In our previous reports,[4,22,23] we have pointed out the importance of the excitonic interactions in organic pigments, in which the absorption coefficient of the component molecule is quite large and the molecules are periodically arranged. When an excitation induces a transition dipole in the molecule, the excited state in crystals involves wave functions with significant probabilities on nearest neighbors. Therefore, the exciton coupling may well involve energy contributions from interactions with all of these nearest-neighbor molecules acting in concert in the lattice. This may lead to a band splitting of the excited state or spectral displacement toward longer wavelengths or shorter wavelengths. The interaction energy ($\Delta E_{\text{exciton}}$) is given by the dipole−dipole equation:[6,7] $\Delta E_{\text{exciton}} = |\mu|^2(1 - 3\cos^2\theta)/r^3$; μ denotes the transition dipole, r the distance between two central points of two dipoles, and θ the angle between the one dipole and the vector connecting the two point dipoles, respectively. As evident from the present equation, the overall spread or shift energy is determined by the strength of the interneighbor coupling ($|\mu|^2$) which directly depends on the absorption coefficient of the molecule as well as the mutual relative orientation of the transition dipoles in molecular assemblies. That is, the term $(1 - 3\cos^2\theta)$ determines the geometrical relationship of transition dipoles correlated with the crystal structure. The bathochromic or hypsochromic shift depends on the critical angle of $\theta = 54.7°$, below which the former will result and above which the latter will be the case. The maximum bathochromic or hypsochromic shift is achieved by head-to-tail arrangement or "parallel" arrangement, respectively.

On the basis of the exciton theory, we will consider the spectral shifts in QA, MMQA, and DMQA with the direction of the transition dipole in mind given in Figure 1. The discussion below is rather crude, but it is of interest and great help for developing an understanding of the exciton coupling effect. As stated in section 3.7, the direction of the transition dipole in γ-QA and MMQA, as determined by experiment, points along the NH···O hydrogen bond. In other words, the hydrogen bonds align the transition dipoles in a head-to-tail fashion (Figures 9 and 10). The present arrangement induces the largest lowering of the excited state, leading to the maximum bathochromic shift upon crystallization. For example, the hydrogen-bond pair in QA is found to cause a large bathochromic shift ($\Delta E_{\text{exciton}}$) of ∼5840 cm^{-1} to occur. (The calculation is based on the transition dipole (μ) computed by the INDO/S Hamiltonian using the *x*, *y*, *z* coordinate set of the X-ray structure analysis.) This clearly indicates that the large bathochromic shift is mainly due to the head-to-tail arrangement of the transition dipole. Similarly, the shift energy amounts to about 2140 cm^{-1}, suggesting that the hydrogen-bond pair is here again responsible for the bathochromic shift. On the other hand, there are no corresponding intermolecular H-bonds in DMQA. Nevertheless, there is a slight bathochromic shift of about 300 cm^{-1}. This is due to the *quasi*-head-to-tail arrangement of the transition dipole between one molecule and the nearest-neighboring one on the (*a*,*c*) plane. Then, we look at the nearest-molecule pair along the stacking axis in γ-QA, MMQA, and DMQA. The interplanar distances and the slip angles (this angle is different from the angle θ between transition dipoles described above) are about 3.39 Å and 61° for γ-QA, 3.39 Å and 63° for MMQA, and 3.35 Å and 43° for DMQA. This shows no significant difference in

geometry between these molecule pairs, suggesting that the spectral shift in γ-QA, MMQA, and DMQA is mainly determined by the head-to-tail arrangement of the transition dipoles.

In summary, the absorption maximum of DMQA (with no hydrogen bond) is less bathochromically displaced than that of MMQA with two hydrogen bonds per molecule. Similarly, QA shows more bathochromic displacement due to four hydrogen bonds per molecule than MMQA. This interprets the extent of the bathochromic shift upon crystallization in γ-QA, MMQA, and DMQA. Then, the major difference in spectral shifts between γ-QA, MMQA, and DMQA can be attributed to the number of NH···O intermolecular hydrogen bonds per molecule.

5. Conclusions

The electronic structure of QA derivatives has been investigated on the basis of the crystal structure, using γ-QA, MMQA, and DMQA with different hydrogen-bond forming characteristics. As for the molecular property of one single molecule, the spectral shift is found to be most sensitive to the electron density at the N atom which can immediately be delocalized in the chromophore. The spectral shift on going from solution to the solid state is most significant in γ-QA, and the extent decreases in the sequence of MMQA and DMQA, respectively. This follows exactly the number of NH···O intermolecular hydrogen bonds. The major intermolecular interaction in DMQA with no hydrogen bond is due to van der Waals one. On the other hand, additional NH···O hydrogen-bond interactions are operative in MMQA with two hydrogen bonds per molecule and in γ-QA with four hydrogen bonds. The hydrogen bonds align the transition dipoles in a head-to-tail fashion to displace the absorption band toward longer wavelengths. This explains the extent of the bathochromic shift upon crystallization in γ-QA, MMQA, and DMQA.

References and Notes

(1) Herbst, W.; Hunger, K. *Industrial Organic Pigments: Production, Properties, Applications*, 3rd ed.; VCH: Weinheim, Germany, 2004.

(2) Mizuguchi, J.; Wooden, G. *Ber. Bunsen-Ges. Phys. Chem.* **1991**, *95*, 1264.

(3) Mizuguchi, J.; Rochat, A. C. *Ber. Bunsen-Ges. Phys. Chem.* **1992**, *96*, 708.

(4) Mizuguchi, J. *J. Phys. Chem. A* **2000**, *104*, 1817.

(5) Mizuguchi, J.; Endo, A.; Matsumoto, S. *J. Imag. Soc. Jpn. (Nippon Gazo Gakkaishi)* **2000**, *39*, 94.

(6) Kasha, M. Molecular Excitons in Small Aggregates. In *NATO Advanced Study Institute Series, Series B*; Bartolo, B. D., Ed.; Plenum Press: New York, 1976; Vol. 12, pp 337−363.

(7) Craig, D. P.; Walmsley, S. H. *Excitons in Molecular Crystals: theory and applications*; W. A. Benjamin, Inc.: New York, 1968.

(8) Potts, G. D.; Jones, W.; Bullock, J. F.; Andrews, S. J.; Maginn, S. J. *J. Chem. Soc., Chem. Commun.* **1994**, 2565.

(9) Mizuguchi, J.; Sasaki, T.; Tojo, K. *Z. Kristallogr.—New Cryst. Struct.* **2002**, *217*, 249.

(10) Mizuguchi, J.; Senju, T. *Z. Kristallogr.—New Cryst. Struct.* **2002**, *217*, 523.

(11) Ohmasa, M.; Süsse, P. *Naturwissenschaften* **1967**, *63*, 387.

(12) Zavodnik, V. E.; Chetkina, L. A.; Val'kova, G. A. *Zh. Strukt. Khim.* **1981**, *22*, 188.

(13) Mizuguchi, J.; Senju, T. *Acta Crystallogr., Sect. E* **2003**, *E59*, o232.

(14) Zambounis, J.; Mizuguchi, J. PCT (Patent Cooperation Treaty) International Application WO 9608536, 1996.

(15) Mizuguchi, J. *Cryst. Res. Technol.* **1981**, *16*, 695.

(16) *Quantum CAChe*, version 3.2; Fujitsu, Ltd.: Kanagawa, Japan, 1999.

(17) Ridley, J.: Zerner, M. *Theor. Chim. Acta* **1973**, *32*, 111.

(18) Süsse P.; Steins, M.; Kupcik, V. *Z. Kristallogr.* **1988**, *184*, 269.

(19) Mizuguchi, J. *Acta Crystallogr., Sect. C* **1992**, *C48*, 1553.

(20) Pauling, L. *The Chemical Bond: a brief introduction to modern structural chemistry*; Cornell University Press: Ithaca, NY, 1967.

(21) Mataga, N.; Kubota, T. *Molecular Interactions and Electronic Spectra*; Marcel Dekker: New York, 1970; Chapter 7.

(22) Mizuguchi, J. *J. Imag. Soc. Jpn. (Nippon Gazo Gakkaishi)* **1998**, *37*, 58.

(23) Mizuguchi, J.; Tojo, K. *J. Phys. Chem. B* **2002**, *106*, 767.